Eur Biophys J (1998) 27: 137–146 © Springer-Verlag 1998

ARTICLE

Flavia Barone · Giuseppe Chirico · Mirella Matzeu
Filomena Mazzei · Francesco Pedone

Triple helix DNA oligomer melting measured by fluorescence polarization anisotropy

Received: 17 July 1997 / Accepted: 22 September 1997

Abstract A synthetic DNA triple helix sequence was formed by annealing a pyrimidinic 21 mer single strand sequence onto the complementary purinic sequence centred on a 27 mer duplex DNA. Melting of the third strand was monitored by UV spectrophotometry in the temperature range 10–90 °C. The T_m of the triplex, 37 °C, was well separated from the onset of duplex melting. When the same triple helix was formed on the duplex bearing one nick in the center of the pyrimidinic sequence the T_m of the triplex was shifted to approximately 32 °C and overlapped the melting of the duplex. We have used fluorescence polarization anisotropy (FPA) measurements of ethidium bromide (EB) intercalated in duplex and triplex samples to determine the hydrodynamic parameters in the temperature range 10–40 °C. The fluorescence lifetime of EB in the samples of double and triple stranded DNA is the same (21.3 ± 0.5 ns) at 20 °C, indicating that the geometries of the intercalation sites are similar. The values for the hydration radii of the duplex, normal triplex, and nicked triplex samples were 10.7 ± 0.2, 12.2 ± 0.2, and 12.0 ± 0.2 Å. FPA measurements on normal triplex DNA as a function of temperature gave a melting profile very similar to that derived by UV absorption spectroscopy. For the triplex carrying a nick, the melting curve obtained using FPA showed a clear shift compared with that obtained for the normal triplex sample. The torsional rigidity of the triplex forms was found to be higher than that of the duplex form.

Key words Triplex DNA · FPA · DNA dynamics

Abbreviations *CD* Circular dichroism · *EB* Ethidium bromide · *EDTA* Ethylene-diamino-tetraacetic acid · *FFT* Fast Fourier transform · *FPA* Fluorescence polarization anisotropy

Based on a presentation at the 2nd European Biophysics Congress, Orléans, France, July 1997

F. Barone · M. Matzeu
Laboratorio di Fisica, Istituto Superiore di Sanità, Roma, Italy

G. Chirico
Istituto Nazionale di Fisica della Materia,
Università degli Studi di Milano, Milano, Italy

F. Mazzei (✉)
Laboratorio di Fisica, Istituto Superiore di Sanità,
Viale Regina Elena 299, I-00161 Roma, Italy
(e-mail: mazzei@iss.infn.it)

F. Pedone
Istituto Nazionale di Fisica della Materia,
Università La Sapienza, Roma, Italy

Introduction

The detection of the decay of the fluorescence anisotropy of DNA intercalated with EB molecules has been applied by several authors (Barkley and Zimm 1979; Schurr et al. 1992; Collini et al. 1995) to the study of DNA dynamics. This approach, applied to long DNA sequences, plasmids and short synthetic oligomers, has been mainly based on the comparison of the experimental data with a comprehensive model of the dynamics of a bendable and twistable rod – the DNA helix – developed by Allison and Schurr (1979).

Recently, Duhamel et al. (1996) have applied a simple model developed by Szabo (1984) to the analysis of FPA studies of short DNA fragments. This model neglects the decay due to bending deformation, which dominates in long DNA samples, and ascribes the anisotropy decay entirely to the torsional motion of the dye. This motion is described by two parameters: the delocalization angle of the dye $\langle l \rangle$, induced by dye twisting coupled to DNA dynamics, and the hydrodynamic radius R_h. One of the aims of the present paper is to show how these simplified models allow one to study mixtures of samples with different forms and to follow transitions among them.

Nucleic acids carry out their biological role by assuming a great variety of forms. The role of DNA sequences which form a triple helix has been investigated since their discovery (Felsenfeld et al. 1957). Synthetic triple stranded

nucleic acid structures can be formed on a homopurine-homopyrimidine duplex by the addition of a third strand of appropriate sequence. This strand is positioned in the major groove and binds to the duplex via Hoogsteen hydrogen bonds. A role for triple helix DNA in chromatin assembly and gene expression has been suggested and structural data have been obtained by a variety of physico-chemical techniques (see Soyfer and Potaman (1996), for a review).

FPA allows one to characterize the nucleic acid structure and to gain information on the hydrodynamic radius and elastic properties of these molecules, by studying the fluorescence of the dye coupled to the DNA motions. Spectrofluorometry of intercalated EB in triplex DNA oligonucleotide, originally performed by Mergny et al. (1991), showed that its binding behaviour in triple helices is similar to that observed in duplex DNA.

DNA interconversion between double and triple strand forms occurs in narrow temperature ranges, in a sequence dependent fashion, but usually with a transition midpoint of 10–15 °C. We have studied the melting transition of a synthetic oligonucleotide triple helix by FPA measurements at temperatures ranging from 10 °C, where EB is intercalated in the triple helix, up to 40 °C, where dissociation of the third strand is complete but EB is still bound to the duplex DNA. The derivation of hydrodynamic parameters as a function of the temperature requires the measurements of the lifetimes of bound EB at various temperatures both in the duplex and triplex DNA forms.

FPA measurements on isolated duplex and triplex samples, in the temperature range 10–25 °C, where these forms are stable, allow one to define the hydrodynamic radii. Thereafter, the residual fraction of triple helix present during a thermal transition in the range 10–40 °C was evaluated and compared with that obtained by conventional UV melting measurements. The reliability of the method has been checked by analyzing another sample which bears a nick and which shows different thermal stability.

Materials and methods

Oligonucleotide preparation

Oligonucleotides:

1) $CGA(TC)_5(T)_{11}AGC$
2) $GCT(A)_{11}(GA)_5TCG$
3) $(T)_{11}(CT)_5$
4) $(T)_{11}AGC$
5) $CGA(TC)_5$

were synthesized using a Beckman SM automated DNA synthesizer. Oligonucleotide length homogeneity was checked by denaturing gel electrophoresis. The fraction of short contaminating fragments was usually less than 3%. The concentration of single strands was determined spectrophotometrically with molar extinction coefficients calculated using nearest-neighbour analysis (Cantor et al. 1970): $\varepsilon_1 = 2.23\times10^5\ M^{-1}\,cm^{-1}$, $\varepsilon_2 = 3.02\times10^5\ M^{-1}\,cm^{-1}$, $\varepsilon_3 = 1.60\times10^5\ M^{-1}\,cm^{-1}$, $\varepsilon_4 = 1.18\times10^5\ M^{-1}\,cm^{-1}$, $\varepsilon_5 = 1.08\times10^5\ M^{-1}\,cm^{-1}$.

In order to obtain the samples shown in Fig. 1, oligonucleotides 1) and 2) (duplex D), 3) and 1) + 2) (triplex T), 3) and 1) + 4) + 5) (nicked triplex nT) were mixed in the appropriate ratio. Annealing was performed by heating the oligonucleotides at 80 °C for 10 min and allowing them to cool down to 4 °C over a 16–18 h period. Annealing, as well as spectroscopic measurements, were performed in 10 mM Na phosphate pH 6.1 buffer, 0.1 mM Na_2EDTA, 200 mM NaCl.

Gel electrophoresis

Samples were electrophoresed on non-denaturing 15% polyacrylamide gels, 30:1 acrylamide/bisacrylamide ratio (17×10×0.075 cm) in Tris-acetate pH 6.1 buffer, 200 mM NaCl at 30 mA for 24 h, 4 °C. The buffer was recirculated during the electrophoresis. DNA bands were visualized by staining with ethidium bromide and photographed under ultraviolet light.

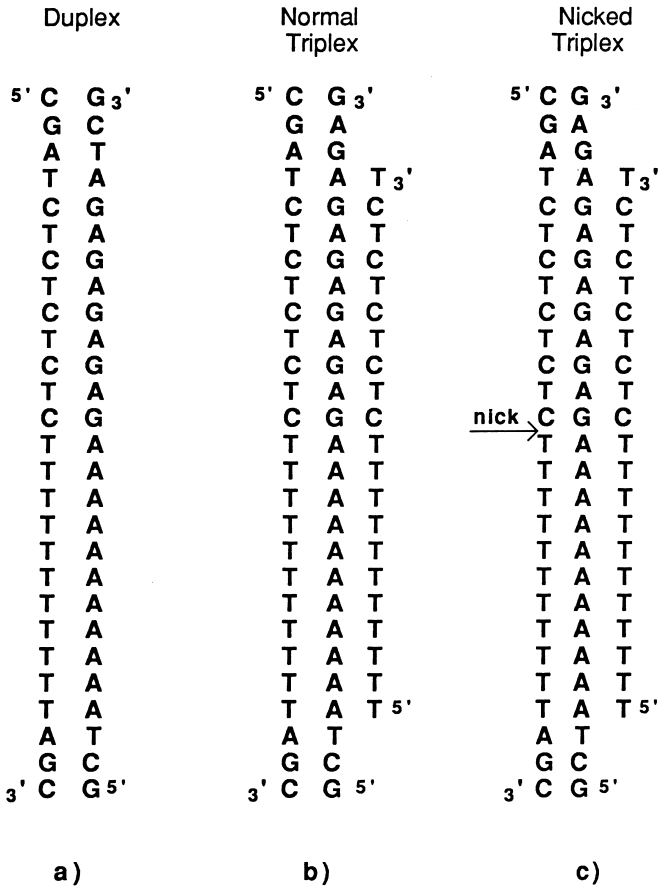

Fig. 1a–c Sequence of the DNA samples. The third strand forms Hoogsteen pyrimidine-purine bonds with parallel orientation. **a** Duplex; **b** normal triplex and **c** nicked triplex

CD measurements

Circular dichroism spectra were recorded between 320 and 200 nm with a Jasco J710 spectropolarimeter. The spectral resolution was 0.2 nm with a band width of 1 nm. The scanning rate was 10 nm/min and every spectrum was the average of two measurements. The samples were thermostated by means of a Haake H20 bath in a cylindrical water-jacketed quartz cell (1 cm optical path length).

UV melting curves

The absorbance at 260 nm as a function of temperature was recorded with a Cary 3 UV/VIS spectrophotometer. Briefly, samples were placed in 1 cm quartz cells and thermostated using a Peltier device that ensured temperature control inside the sample cell to within 0.1 °C. The temperature was increased at a rate of 0.5 °C/min and data points were recorded every 0.2 °C. Absorbance values, corrected for the thermal expansion of water and normalized to A_{260} = 1 at the lower temperature, were plotted against temperature. When the transitions were well separated in the absorbance profiles, the fraction of triplex samples (α_T) was calculated by the ratio:

$$\alpha_T = \frac{A_{max} - A_T}{A_{max} - A_{min}}$$

where A_{max} and A_{min} are the absorbance values at 44° and 4 °C respectively and A_T is the absorbance value at the temperature T.

Dynamic fluorescence measurements

Lifetimes and fluorescence polarization anisotropy measurements were performed on a K2-ISS phase-shift fluorometer (Urbana Illinois, USA) using the 514 nm 0.5 W output of a Spectra Physics 165 CW argon laser. The modulation ratio of the excitation light was always in the range 60–70% and the detection cross correlation frequency was 80 Hz (see Gratton 1984 for further technical details).

Samples were placed in 1 cm quartz cells and a long pass filter (550 nm) was placed between the sample turret and the photomultiplier to minimize detection of scattered light. For the lifetime measurements 10 frequencies logarithmically spaced in the 2–40 MHz interval were acquired. The excitation polarizer was set at 35° and a polystyrene lattice was used as the reference. In the FPA measurements 20 frequencies were acquired in the 2–40 MHz interval with the excitation polarizer kept fixed at 0° (i.e. vertical) and the emission polarizer periodically and automatically rotated to 0° and 90° for each acquisition. The differences between the phase shifts and the ratios between the modulation ratios measured for the two positions of the polarizer and the analyzer characterize the fluorescence anisotropy as discussed in the following section. The errors for the phase and modulation were 0.2° and 0.004 respectively, amounting to ≅1% of the signal. The temperature of the samples was controlled by means of a circulating water bath (Haake K15) in the range 10–40 °C. The stability of the temperature to within 0.5 °C was checked before and after each acquisition. The DNA samples were dissolved in Na phosphate pH 6.1 buffer, 200 mM NaCl. Ethidium bromide (2,7-diamino-10-ethyl-9-phenylphenanthridinium bromide) was from Boehringer and was dissolved in the same buffer at a fixed concentration of about 1 mM.

To avoid energy transfer processes between intercalated dye molecules the DNA base pair/EB ratio and DNA base triplet/EB ratio were usually greater than 200.

The data were analyzed with the ISS fluorometer software for lifetime determination and with a Vax for the anisotropies.

Theory

The computation of the fluorescence anisotropy decay for a realistic DNA model has been given by Allison and Schurr (1979). The DNA helix is imagined as a bendable and twistable set of N + 1 stacked cylinders which represent the base pairs. In general, the fluorescence anisotropy is given by products (Schurr 1984) of internal geometric factors $A_n(t)$ for the particular dye intercalating geometry, and of bending $F_n(t)$ and torsional $C_n(t)$ correlation functions:

$$r(t) = \frac{(I_{\parallel} - I_{\perp})}{(I_{\parallel} + 2I_{\perp})} = r_0 \sum_{n=-2}^{2} A_n(t)\, C_n(t)\, F_n(t) \qquad (1)$$

where r_0 is the initial anisotropy value, assumed to be 0.36 for the dye wobbling (Millar et al. 1982). The internal correlation functions $A_n(t)$ are related to the angle θ formed by the EB dipole and the helix axis, assumed to be 70.5° (Schurr 1984):

$$A_0 = \left(\frac{3}{2}\cos^2\theta - \frac{1}{2}\right)^2;\ A_1 = 3\cos^2\theta\sin^2\theta;\ A_2 = \frac{3}{4}\sin^4\theta$$

The torsional correlation functions $C_n(t)$ are related to the relaxation time τ_l of the lth normal mode and to its corresponding mean square amplitude d_l^2 by:

$$C_n(t) = (N+1)^{-1}\exp(-n^2 D_{\parallel} t) \sum_{m=1}^{N+1} \exp\left[-n^2 \sum_{l=2}^{N+1} d_l^2\, Q_{ml}^2 \left(1 - e^{-t/\tau_l}\right)\right] \qquad (2)$$

where Q_{ml} is the element of the normal mode transformation matrix associated with the lth normal mode and to the mth subunit as reported by Schurr (1984). These quantities are given by:

$$\tau_l = \frac{\gamma}{4\alpha\sin^2\left[(l-1)\pi/[2(N+1)]\right]};$$

$$d_l^2 = \frac{k_B T}{4\alpha\sin^2\left[(l-1)\pi/[2(N+1)]\right]};$$

$$Q_{ml} = [2/(N+1)]^{\frac{1}{2}} \cos\left[\left(m-\frac{1}{2}\right)(l-1)\pi/(N+1)\right];$$

$$\gamma = \frac{k_B T}{D_{\parallel}(N+1)}$$

where α is the DNA torsional constant which is related to the torsional rigidity C and to the base pair height b = L/(N + 1) through α = C/b.

For a straight fragment, the rotational diffusion coefficients can be computed by assuming that the DNA behaves as a straight cylinder of length L and radius R, i.e. (Tirado and Garcia de la Torre 1980):

$$\begin{aligned} D_{\parallel} &= k_B T \Big/ \left[(3.8441)\pi\eta L R^2 (1+\delta_{\parallel})\right]; \\ D_{\perp} &= 3k_B T(\ln p + \delta_{\perp})/\pi\eta L^3 \\ \delta_{\parallel} &= (0.677/p) - (0.183/p^2); \\ \delta_{\perp} &= -0.662 + (0.917/p) - 0.05/p^2 \end{aligned} \tag{3}$$

where p = (L/2R), T is the absolute temperature and η is the solution viscosity.

The bending correlation functions $F_n(t)$ are expressed according to:

$$F_n(t) = \exp\left[-(6-n^2)D_{\perp}t\right] \cdot \exp\left[-(6-n^2)A_n \sum_{k=l}^{k_{\max}} \frac{(1-e^{-t/T_k})}{(2k+1)^2}\right] \tag{4}$$

where

$$A_n = \frac{-\ln D_n(\infty)}{\left[(6-n^2)\sum_{k=1}^{k_{\max}} \frac{1}{(2k+1)^2}\right]}$$

and

$$D_n(\infty) = (Z_n)^{-1/2} \exp(-Z_n/3)\left(\pi^{1/2}/2\right) erf\left(Z_n^{1/2}\right)$$

and $Z_n = (6-n^2)L/4P$; erf is the error function.

$$\frac{1}{T_k} = \frac{k_B T P k_k^4}{4\pi\eta}\left[K_0(k_k R_H) + \left(\frac{k_k R_H}{2}\right)K_1(k_k R_H)\right]$$

$$\text{and} \quad k_k = \frac{(2k+1)\pi}{2L}$$

The maximum number of relaxation bending modes, $k_{\max}$, was chosen as the index k for which $T_{k+1} > T_k$ and was typically equal to 10. The dynamic persistence length P was computed from the bending rigidity A according to: P = A/(KT).

More recently, Duhamel et al. (1996) have shown that for short polynucleotide fragments (6-32 base-pairs) one can satisfactorily describe the FPA data by means of a simpler dynamic model proposed by Szabo (1984). In this picture one considers the short DNA fragment as a rigid rod endowed with a proper rigid body rotational diffusion coefficient. The depolarization of fluorescence arising from the motion of the dye coupled to the base-pair twisting is described by rotational diffusion of the dye between two reflecting barriers at an angle $\langle l \rangle$. The further assumptions of the model are: (1) the dye wobbling inside the intercalation pocket and the base-pair twisting are independent internal motions, and (2) the internal bending motions can be disregarded for such short DNAs. The bending correlation functions are therefore assumed to be $F_n(t) = e^{-(6-n^2)D_{\perp}t}$, while the torsional correlation functions are given by the product of the rigid body spinning diffusion motion and the internal torsional motion of the dye inside the binding pocket:

$$C_n(t) = e^{-n^2 D_{\parallel} t} I_n(t) \tag{5}$$

where:

$$I_0 = 1 \quad I_1 = \left(\frac{\sin(\langle l \rangle/2)}{(\langle l \rangle/2)}\right)^2 \quad I_2 = \left(\frac{\sin(\langle l \rangle)}{\langle l \rangle}\right)^2$$

The θ appearing in the definition of the $A_n(t)$ (Eq. (1)) is again the angle between the dye dipole moment and the axis around which the rotational motion of the dye occurs. This model allows the computation of the FPA decay as a sum of simple exponential decays:

$$\begin{aligned} \frac{r(t)}{r_0} &= \frac{1}{4} e^{-6D_{\perp}t}\left(3\cos^2(\theta) - 1\right)^2 \\ &+ 3I_1 e^{-(5D_{\perp} + D_{\parallel})t} \sin^2(\theta)\cos^2(\theta) \\ &+ \frac{3}{4} I_2 e^{-(2D_{\perp} + 4D_{\parallel})t} \sin^4(\theta) \end{aligned} \tag{6}$$

where tumbling and spinning diffusion coefficients can be computed according to Tirado and Garcia de la Torre (see Eq. (3)). One can easily perform the analytical Laplace transform of the intensity decays $I_{\parallel}(t)$, $I_{\perp}(t)$ needed to compute the phase shifts and the demodulation ratios, measured with the frequency modulated excitation light. However, this simplified picture of DNA dynamics should be compared to the more realistic one developed by Allison and Schurr (1979). This has been partially performed by Duhamel et al. (1996) and will be extended in the Results section to the case of different torsional constants and persistence lengths.

In the presence of several dye species, the contribution of each of these to the decay of fluorescence anisotropy is summed in the total anisotropy, weighted by the corresponding fluorescence intensity

$$r(t) = \frac{\sum_{i=1}^{M}\left(\frac{x_i}{\tau_i}\right)e^{-t/\tau_i} r_i(t)}{\sum_{i=1}^{M}\left(\frac{x_i}{\tau_i}\right)e^{-t/\tau_i}} \tag{7}$$

where x_i, τ_i and $r_i(t)$ are the fractional intensities, the fluorescence lifetime and the anisotropy of the i-th species re-

spectively computed with some model for the DNA dynamics. We assume here a single lifetime decay for the fluorescence of each species, as experimentally confirmed (see Results).

In the present study of triple helix melting, one expects to have the following fractions in solution (1) free ethidium, x_f, (2) ethidium bound to DNA double helices, x_D, and (3) ethidium intercalated DNA triple helices, x_T. One might also think of a small contribution from ethidium bound to melted single strands.

Both in the numerical simulations and in the data fitting, the free dye anisotropy contribution was described by a single exponential decay $r_f(t) = r_{0f} e^{-t/\tau_f}$, where $r_{0f} = 0.4$ and $\tau_f = 100$ ps (Madge 1983). The computed anisotropy time decays were converted into the measurable quantities, i.e. the fluorescence phase shift differences $\Delta(\omega) = \Phi_\perp(\omega) - \Phi_{||}(\omega)$ and the demodulation ratios $\Lambda(\omega) = M_{||}/M_\perp$ as suggested earlier by Weber (1977).

The Laplace transform of the time decay of the fluorescence intensity as measured when the relative orientation of the excitation polarizer and the emission analyzer are parallel, $I_{||}(t) = I_{tot}(t)(1 + 2r(t))$, and orthogonal, $I_\perp(t) = I_{tot}(t)(1 - r(t))$ are:

$$f_p(\omega) = \int_0^\infty dt I_p(t) e^{i\omega t} = L(I_p)(i\omega) \tag{8}$$

where p = || or p = ⊥ were computed and combined as:

$$\Lambda(\omega) = |f_\perp(\omega)| / |f_{||}(\omega)|$$
$$tg(\Delta(w)) = \frac{\mathrm{Im}(f_\perp)\mathrm{Re}(f_{||}) - \mathrm{Re}(f_\perp)\mathrm{Im}(f_{||})}{\mathrm{Re}(f_\perp)\mathrm{Re}(f_{||}) + \mathrm{Im}(f_\perp)\mathrm{Im}(f_{||})} \tag{9}$$

The Laplace transform of Duhamel's model (Eqs. (1) and (6)) was easily computed analytically while that of Schurr's model (Eqs. (1), (2) and (4)) needed a numerical FFT procedure.

Results

Sample characterization

The study described here has been performed on purified and well characterized triple helix DNA. Proper annealing of the three strands was checked by electrophoretic analysis and circular dichroism measurements. In Fig. 2 the electrophoretic pattern of samples obtained by adding to the normal duplex form an increasing amount of the third strand and annealing them as described in Methods section are reported. The resulting samples are shown in lanes 1–4, where the formation of the slower migrating band of the triplex is evident. This reduced mobility is due to the increased molecular weight and stiffness of the triplex DNA form. In lane 4 the addition of a stoichiometric amount of the third strand results in the complete formation of the triplex. The samples of Fig. 2 were analyzed by circular dichroism and the resulting spectra are shown in Fig. 3.

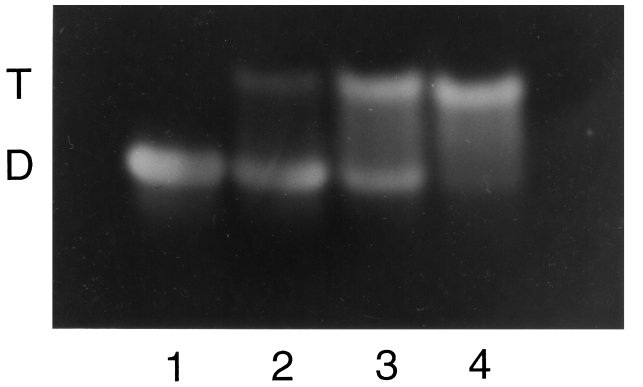

Fig. 2 Electrophoretic patterns of DNA duplex and triplex. 15% polyacrylamide gel electrophoresis run in Tris acetate buffer, 200 mM NaCl, pH 6.1 at 30 mA for 24 h, at 4 °C, *Lane 1* contains duplex sample; *lanes 2–4* contain the reaction products of the annealing of the duplex sample with the third strand at ratios 1:0.24, 1:0.5 and 1:1 respectively

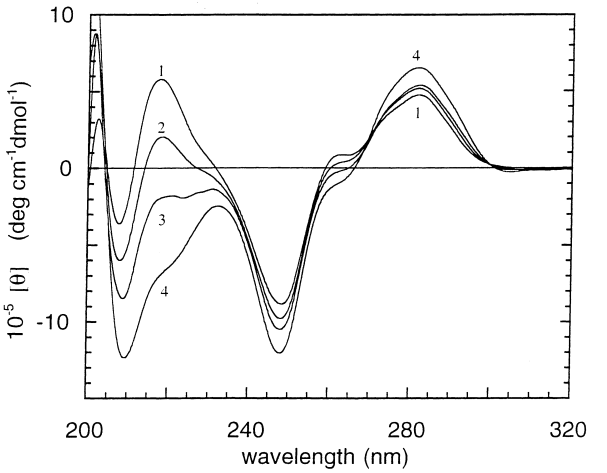

Fig. 3 Circular dichroism spectra of duplex and triplex DNA samples at 10 °C. The samples at 1.7 10^{-4} M, were thermostated in a cylindrical water-jacked quartz cell, 1 cm path length. Spectra were recorded at a rate of 10 nm/min with a spectral resolution of 0.2 nm and a band width of 1 nm. 1) duplex DNA; 2, 3, 4) duplex/third strand at molar ratios of 1:0.24, 1:0.5, and 1:1, respectively

The gradual formation of triplex is mainly evident in the 200–230 nm region of the spectra through a decrease in ellipticity at 209 and 220 nm. Minor changes occur in the higher wavelength range of the spectra which assume the usual duplex form. In the spectra the sharp shoulder around 265 nm, characteristic of poly dA-poly dT and of A-form containing DNAs (Gray et al. 1992) is evident. A reduction in ellipticity at this wavelength is observed following triplex formation, in agreement with results reported elsewhere (Manzini et al. 1990). A similar procedure was carried out for the annealing and characterization of the nicked triplex (data not shown).

Figure 4 shows the absorbance UV melting profiles of the normal and nicked triplex samples. In the normal sam-

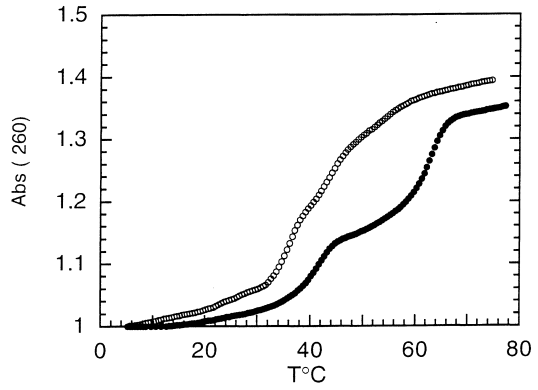

Fig. 4 UV melting absorbance profiles of triplex samples. ● Normal triplex and ○ nicked triplex. Absorbance values at 260 nm were normalized to an optical density of 1 at 260 nm. Correction factors for thermal expansion were taken into account

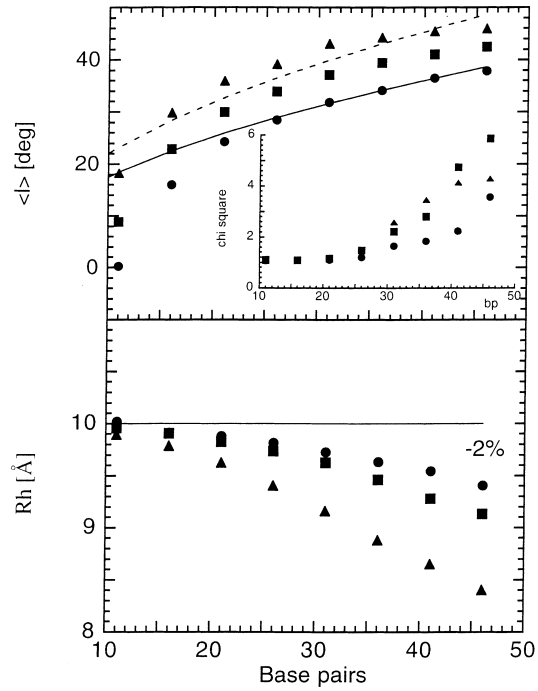

Fig. 5 Delocalization angle $\langle l \rangle$ and hydrodynamic radius R_h from the Duhamel fit of simulated data with $\alpha = 5\times10^{-12}$ erg, P = 200 nm (■); $\alpha = 5\times10^{-12}$ erg, P = 50 nm (▲) and $\alpha = 8\times10^{-12}$ erg, P = 200 nm (●). The continuous and dashed lines correspond to the torsional contribution $\langle l_{TOR} \rangle$ to the delocalization angle (see Eq. (10)) with $\alpha = 8\times10^{-12}$ erg and $\alpha = 5\times10^{-12}$ erg respectively. The inset shows the normalized χ^2 values and the solid line in the lower plot indicates the simulation value of $R_h = 10$ Å

ple the triplex to duplex and duplex to single strand transitions are well separated and T_m values of 37° and 60 °C, respectively, can be derived. In the nicked sample the two transitions overlap and we cannot assign T_m values to the duplex and triplex components. As previously observed (Bonincontro et al. 1993, Barone et al. submitted paper) the introduction of a nick in the duplex strongly destabilizes the DNA structure, and the melting of the triplex is only slightly affected.

FPA simulations

The assumptions leading to the simple Duhamel model need to be checked against a realistic model for DNA dynamics, which we assume to be the one developed by Allison and Schurr (1979) summarized in Materials and Methods. The aim is to assess the reliability of the simpler Duhamel model for fitting FPA data from multi-component solutions such as those expected during melting transitions. The general procedure consists in the simulation of FPA decays for single or two-component solutions of polynucleotides by Schurr's model (Eqs. (2), (4)) and their subsequent fitting to a single or two-component Duhamel's model (Eq. (6)). In the following the limiting anisotropy and the angle between the dye dipole and the DNA axis were kept at $r_0 = 0.36$ and $\theta = 70.5°$ in both simulations and fitting.

FPA decays for single component solutions of double stranded DNAs were simulated according to Schurr's model. The simulation parameters were: DNA radius $R_h = 10$ Å, torsional constant $5 < \alpha < 8\times10^{-12}$ erg, dynamic persistence length $50 < P < 200$ nm and number of base pairs $10 < N < 50$. Different values of Poisson noise were added to simulated data. The phase shift differences $\Delta(\omega)$ and demodulation ratios $\Lambda(\omega)$ were then computed according to Eq. (9) from the time decay of the fluorescence intensities and the simulated FPA data were fitted to Duhamel's model for one polynucleotide species by keeping as fitting parameters R_h and the dye delocalization angle $\langle l \rangle$. The results of the simulations performed for different values of α and P, averaged over the different values of the added Poisson noise are summarized in Fig. 5. The fitting is usually successful for $N \leq 30$, as judged from the χ^2 value, and depends on the extent of the DNA flexibility: for P = 200 nm and $\alpha = 8\times10^{-12}$ erg the fitting is satisfactorily up to $N \cong 40$. The best fit hydrodynamic radius R_h is always found within 10% of the simulation value; however, when assuming $P \cong 200$ nm and $\alpha \cong 8\times10^{-12}$ erg, agreement within ≅3% is found in the range $10 < N < 30$.

In order to assess the relative contribution of the torsional and bending internal motions to the amplitudes I_1 and I_2 (Eq. (5)) of Duhamel's model, a comparison with what is predicted by Schurr's model for the internal torsional dynamics alone, is interesting.

The torsional contribution to the delocalization angle $\langle l_{TOR} \rangle$ can be estimated by inverting either of the two relations:

$$\left(\frac{\sin\left(\langle l_{TOR}\rangle\right)/2}{\left(\langle l_{TOR}\rangle/2\right)}\right)^2 = (N+1)^{-1}\sum_{m=1}^{N+1}\exp\left[-\sum_{l=2}^{N+1} d_l^2\, Q_{ml}^2\right]$$

$$\left(\frac{\sin\left(\langle l_{TOR}\rangle\right)}{\langle l_{TOR}\rangle}\right)^2 = (N+1)^{-1}\sum_{m=1}^{N+1}\exp\left[-4\sum_{l=2}^{N+1} d_l^2\, Q_{ml}^2\right] \qquad (10)$$

The two estimates of $\langle l_{TOR} \rangle$ obtained by inverting the previous equations agree within ≅1% for torsional constants $\alpha = 5 - 8 \times 10^{-12}$ erg. The delocalization angle increases with the length (Fig. 5) and decreases with α, reflecting the reduced torsional mobility experienced by the dye. The comparison of $\langle l_{TOR} \rangle$ to the best fit values of the simulated data, shows that for lower torsional rigidities the effect of the bending motion on $\langle l \rangle$ is not negligible (Fig. 5). Good agreement between $\langle l \rangle$ and $\langle l_{TOR} \rangle$ is found for relatively rigid DNAs, $\alpha = 8 \times 10^{-12}$ erg, while for $\alpha = 5 \times 10^{-12}$ erg neither the simulated data at P = 200 nm or those at P = 50 nm are quantitatively described by the torsional contribution $\langle l_{TOR} \rangle$. These results make us confident that Duhamel's model can be used to satisfactorily describe FPA data on short (<30 bp base pairs) DNA fragments and allows an accurate determination of their radii. However, information on DNA torsional and bending rigidity are not as directly obtainable as the radius R_h, since depolarization due to DNA flexibility is described by a single parameter: the dye delocalization angle $\langle l \rangle$.

The ability of Duhamel's model to describe FPA data for a two-component solution was verified by numerically simulating FPA decays of a mixture of two DNA fragments of the same length but different radii: $R_D = 11$ Å and $R_T = 12.6$ Å. As discussed in the following section, these values are within the range of our best experimental estimates of the double and triple helix radii. The total anisotropy was computed by means of Eq. (7) with M = 2 and Schurr's anisotropies for the two species (Eq. (2), (4)). The fluorescence lifetimes for the dye bound to the two species were $\tau_D = \tau_T = 22.5$ ns and fractions of the D species were $x_D = 0, 20, 40, 60, 80, 100\%$ ($x_D + x_T = 1$): no free dye contribution was considered. The elastic parameters for DNA were kept at $\alpha = 8 \times 10^{-12}$ erg, P = 200 nm.

The simulated data for different fractions of species D were first fitted to a single species Duhamel model (see Eq. (6)) to obtain an average polynucleotide radius $\langle R_h \rangle$ and a delocalization angle $\langle l \rangle$. In Fig. 6 (upper panel) $\langle R_h \rangle$ is plotted versus the simulation value of x_D showing a smooth decrease from the value $\langle R_h \rangle \cong R_T$ to the value $\langle R_h \rangle \cong R_D$. The values of the hydrodynamic radius for $x_D = 0$ and $x_D = 100\%$ averaged over the different levels of Poisson noise added to the data are $\langle R_h \rangle = 12.6 \pm 0.2$ Å and $\langle R_h \rangle = 11.0 \pm 0.3$ Å respectively. The delocalization angle showed no clear trend versus x_D as can be expected since the simulation values of the elastic polynucleotide parameters were the same for the two species.

The same set of simulated data was then fitted to a population of two species of polynucleotides described by Duhamel's model (see Eq. (6)). Possible free parameters for this fit are the hydrodynamic radii, the delocalization angle for the two species and the fractions of the D species x_D. However, in order to reduce the number of fitting parameters, for each level of added Poisson noise, a single species fit (i.e. M = 1 in Eq. (7)) to the $x_D = 100$ and $x_D = 0\%$ data sets was first performed. The two values of the best fit hydrodynamic radii, R_D^{fit}, R_T^{fit} and delocalization angles $\langle l \rangle_D^{fit}$, $\langle l \rangle_T^{fit}$ were identified with those for the T ($x_D = 0\%$) and D ($x_D = 100\%$) species and kept fixed in the subsequent

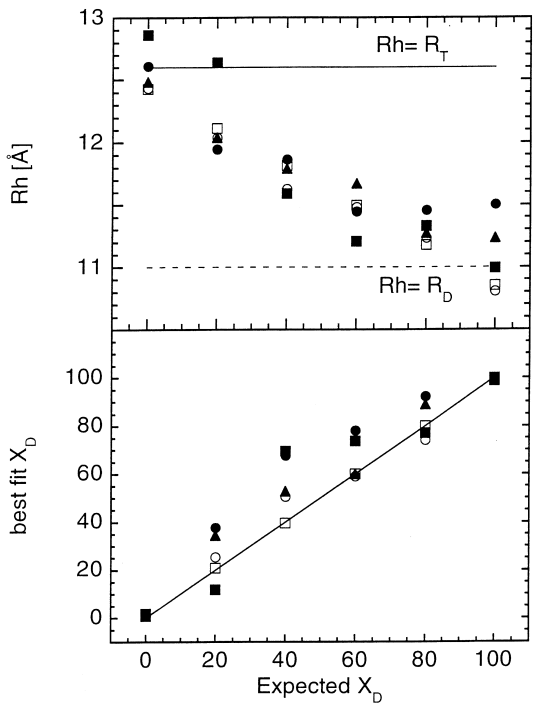

Fig. 6 Fits of the simulations of the two-component solution ($\alpha = 8 \times 10^{-12}$ erg, P = 200 nm) versus the D species simulation fraction x_D. The upper panel shows the best fit hydrodynamic radius R_h obtained from the single-component Duhamel fit for different levels of added Poisson noise: □ 0.1%, ○ 1.6%, ▲ 3.2%, ● 4.5%, ■ 6.4%. The lower panel shows the best fit value of the x_D fractions obtained from a two-components Duhamel's fit: symbols refer to the same added Poisson noise levels as in the upper panel

fit of the simulated data in intermediate values of x_D with the two species model. The best fit values of the D fraction, x_D, versus their corresponding simulation values are plotted in Fig. 6 (lower panel) for different levels of added Poisson noise. The results are very satisfactory at least for a noise level up to 1.6%, which is higher than the typical experimental level (≅1%). This agreement does not change substantially when the delocalization angle $\langle l \rangle_T$ is allowed to be an additional free parameter in the fit.

Finally, we considered the effect of some statistical or systematic error on the estimates of R_D^{fit}, R_T^{fit} on the fitting result. The fitting procedure described above was performed while keeping the D and T species radii at values slightly different from R_D^{fit}, R_T^{fit}, i.e. the ones obtained from a single component fit to the data sets at $x_D = 0$ and 100%. The average difference between the best fit and the simulation values of x_D was found to be always ≤7% when the error on the estimates of the radii was ≤2% and one could reach 20% average difference when the error of the radii was as high as 7–10%. This showed that the typical experimental error (≅1%) in the estimate of R_D^{fit}, R_T^{fit} induces at most an uncertainty ≅5–6% in the evaluation of the fractions of the two components.

FPA measurements

The determination of the polarization anisotropy of EB bound to duplex and triplex samples requires the knowledge of the respective lifetimes. They were measured at various temperatures in the range 10–35 °C for the duplex, and in the range 10–20 °C for the normal triplex sample. The values at 20 °C obtained for the duplex are 21.3 ± 0.5 ns for the bound form and 1.7 ± 0.2 ns for the free form. The temperature dependence of the lifetime of the bound form was fitted by linear regression and was accounted for in the anisotropy fitting procedures. The lifetime at 20 °C of EB bound to the triplex was 21.2 ± 0.5 ns, similar within error to that of the duplex. Its temperature dependence was $\tau_B = -0.00458T - 0.0039$.

In Fig. 7, the phase shift ($\Delta\phi$) and modulation ratio (Λm) measured at 20 °C for duplex and normal triplex samples in the frequency interval 2–40 MHz are reported; the continuous lines are the best fit obtained according to Schurr. Some differences are readily distinguishable in the curves obtained for these samples. The single strand phase shift and demodulation ratio were measured as a control and are reported in the same figure. The sequence of the single strand has been designed in order to avoid the formation of secondary structures and we have measured a very low level of EB binding to this form. As reported in the legend the amount of single strand present in the FPA measurement is about one third of the mass of the triplex and has been adopted to simulate the complete dissociation of the triplex.

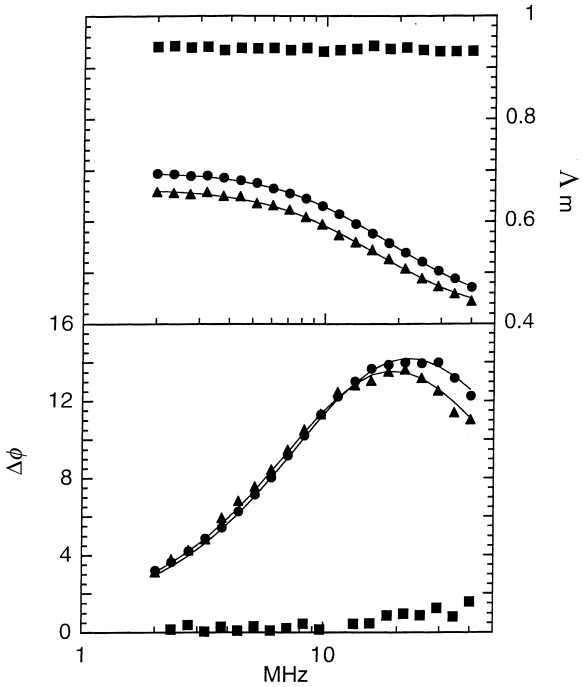

Fig. 7 Phase shift (lower part) and modulation ratio (upper part) at 20 °C, as a function of the frequency of single third strand (■), duplex (●) and normal triplex samples (▲). The continuous curves are the best fit curves obtained according to Schurr's model. The amount of single third strand (■) was 1.4×10^{-4} M

FPA measurements were carried out for duplex, normal triplex and nicked triplex at various temperatures and fitted according to the Schurr or Duhamel models. The values of R_h and $\langle l \rangle$ are reported in Table 1. The R_h of the duplex obtained with both models is smaller than that of the triplex forms based on the expected increase in diameter after the annealing of the third strand. The mean values of 11 Å obtained using Schurr's model and 10.7 Å obtained using Duhamel's fitting procedure for one component are in the range of the values reported in the literature for short DNA fragments in solution (Fujimoto et al. 1994, Nuutero et al. 1994, Duhamel et al. 1996). The R_h of short synthetic DNA oligonucleotides in normal triplex form and in the nicked triplex, which has never been previously reported, were found to be equal to 12.2 Å and 12.0 Å respectively with Duhamel's model. The minor difference (3%) in the R_h obtained using Schurr and one component Duhamel models correlates well with what is observed by FPA simulations (see Fig. 5).

At low temperature, where the conformation of each sample is well defined and differentiated, marked differences in the torsional constant α and in the rotational diffusion angle $\langle l \rangle$ were observed in the three samples. Both parameters are related to the relative motions of base pairs or triplets in the duplex or triplex form of DNA. Higher values of α, characteristic of more rigid structures, and a lower $\langle l \rangle$ value, the signature of a reduced diffusional mobility, observed in both normal and nicked triplex indicate that these samples have a stiffer structure compared to the duplex. FPA measurements carried out on well characterized DNA samples can show, by analysis of the torsional rigidity, subtle differences in conformation, such as those due to the breakage of one strand. In fact, in Table 1 it is shown that the normal triplex at 10 °C has a higher α value of $6.6\pm0.3\times10^{-12}$ erg that decreases to $5.7\pm0.3\times10^{-12}$ erg for the nicked samples. A linear decrease of α with temperature was observed in all three samples. At the present, we can not easily explain such behaviour, but it is certainly not correlated with the thermal stability of the duplex, which is confirmed by the constancy of its hydrodynamic radius with temperature up to about 40 °C.

The R_h values of the triplex samples obtained by fitting with the Schurr and the one component Duhamel models decrease with temperature. This trend is due to the transition of the triplex to the duplex form and in order to weight their relative amount the experimental data were fitted with the two component Duhamel procedure. This model takes into account the presence of two species: triplex and duplex, with intercalated EB. At 10 °C a single species is present, the triplex form, but on increasing the temperature the relative amount of the two species varies; near 40 °C almost all the triplex has became duplex. The mixture model requires the introduction of some fixed parameters. The $\langle l \rangle$ values for the duplex at various temperatures were taken from Table 1 and the R_h of duplex and triplex, averaged in the range 10–20 °C, were 10.7 Å and 12.2 Å respectively. We have assumed these values to fit the re-

Table 1 Parameters derived by fitting FPA data according to Allison and Schurr (1979) with $r_0 = 0.36$ and $A = 8.22$ or Duhamel et al. (1996) with $r_0 = 0.36$ and $\theta = 70.5°$; in the two component model $R_{hD} = 10.7$ Å, $R_{hT} = 12.2$ Å and $R_{hnT} = 12$ Å were fixed

Sample	T°C	Schurr		Duhamel			
				One component		Two components	
		R_h (Å)	$\alpha \cdot 10^{-12}$ (erg)	R_h (Å)	$\langle l \rangle$	$\langle l \rangle_T$	x_T
Duplex	10	11.1	4.2	10.7	37.5	–	–
„	12.4	11.0	3.8	10.6	39.1	–	–
„	14.5	11.0	3.8	10.7	39.3	–	–
„	16	11.0	3.6	10.6	40.0	–	–
„	18	11.1	3.4	10.8	41.1	–	–
„	20	11.1	3.3	10.7	41.7	–	–
„	22.6	11.2	2.8	10.7	44.0	–	–
„	24.6	11.0	2.9	10.6	43.3	–	–
„	30.3	11.1	2.6	10.7	45.6	–	–
„	37.5	11.4	1.9	10.8	50.5	–	–
Normal triplex	10	12.5	6.6	12.2	32.4	32.2	1
„	15	12.4	5.6	12.1	34.6	34.1	0.94
„	20	12.5	4.5	12.1	37.5	37.3	0.96
„	25	12.4	4.2	12.0	38.6	37.7	0.89
„	30	12.1	3.1	11.6	43.0	40.2	0.61
„	35	11.8	2.7	11.4	44.8	38.1	0.42
„	40	11.6	1.7	11.0	52.3	56.8	0.18
Nicked triplex	10	12.3	5.7	12.0	34.1	33.9	0.98
„	15	12.1	5.0	11.8	35.9	34.9	0.84
„	20	12.3	4.3	11.9	38.3	37.9	0.94
„	25	11.7	3.5	11.3	40.9	36.4	0.48
„	30	11.6	3.0	11.2	43.5	38.1	0.41
„	35	10.8	2.1	10.3	49.2	45.1	0
„	40	10.4	1.5	9.8	55.3	–	–

sidual fraction and the $\langle l \rangle$ values of normal triplex at the various temperatures (Table 1).

The same fitting procedure was used to calculate the residual fraction of the nicked triplex form versus T, after verifying that the hydrodynamic radius of the nicked duplex has the same value as the intact duplex form (data not shown). The temperature interval was limited to 30 °C owing to the greater instability of this form and to the higher values of χ^2 (>1.2) obtained by fitting with the mixture model beyond this temperature. The R_h value of the nicked triplex used in the fit was 12.0 Å (Table 1), as obtained in the temperature range 10–20 °C. The residual fractions of the normal and nicked triplex as a function of the temperature are reported in Table 1 and plotted in Fig. 8 together with the residual fraction of the normal triplex form, obtained by the analysis of UV melting data. In this figure a shift of the melting temperature of the nicked triplex sample toward lower temperatures is evident. In particular it must be pointed out that at 25 °C the value of the normal triplex residual fraction is still near unity, whilst that of the nicked form is strongly reduced. A graph of the residual fraction of the nicked triplex sample obtained from the UV melting data, has not been reported because of the overlapping of the duplex and triplex transitions. It is, however, evident that the difference in T_m of the two triplex forms is well represented by the FPA thermal analysis. Finally we note that some differences beyond 25 °C are observed between UV and FPA profiles for the triplex sample; these could be due to slight hysteresis phenomena related to the heating rate we used in the absorbance experiments. We have observed by UV melting measurements on a similar triplex structure that a reduction of the heating rate from 0.5 °C/min to 0.1 °C decreases the melting temperature by about 2 °C (data not shown).

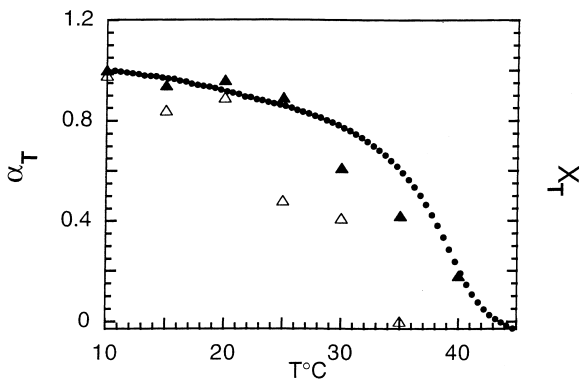

Fig. 8 Triple helix residual fraction vs temperature. Residual fraction of ▲ normal and △ nicked triple helix DNA evaluated from FPA measurements and ● normal triplex deduced from UV melting data

Conclusions

Using FPA measurements we have been able to calculate the residual fraction of triplex during its melting transition in the temperature range 10–40 °C. Moreover, the estimated relative amount of the triplex and duplex species is in good agreement with that obtained from the corresponding UV melting curve, suggesting the possibility of using FPA analysis to accurately monitor conformational variation in DNA samples. With the FPA analysis we discriminate melting temperature differences of about 5 °C, as observed by the comparison of normal and nicked triplex samples.

FPA in comparison with conventional UV spectroscopy yields structural and dynamic information. We have estimated differences in the hydrodynamic radius of our samples ranging from 12.2 to 10.7 Å. Literature data derived by X-rays analysis on RNA and DNA triple helix fibers (Arnott et al. 1973, Liu et al. 1994) and theoretical calculations (Raghunathan et al. 1993) show a displacement of the triple helix axis with respect to that of the double helix, with a concomitant increase of the triplex diameter by 3 Å. Our data are consistent with these findings and confirm that the third strand in a triple helix is deeply buried in the major groove of the duplex.

The torsional rigidities of our triplex DNA oligonucleotides are higher than those of the corresponding duplexes. Millar et al. (1982), using time resolved fluorescence spectroscopy, reported a value of 1.9 for the ratio of the torsional rigidity of a poly(dA) · poly(rU) · poly(rU) triplex to that of duplex DNA. We obtain a smaller triplex to duplex ratio of the torsional constant (α) equal to 1.2. This difference can be ascribed to the different nature of the samples, i.e. DNA or RNA-DNA hybrid triplex, but the increase in stiffness of the triplex due to the association of the third strand with the duplex DNA is confirmed. Finally we note that torsional rigidity is affected by the introduction of one single-strand breakage and the difference is readily detected by FPA measurements.

Acknowledgements We would like to acknowledge Tomasino Pace for synthesizing the oligonucleotides. This research has been partially supported by the National Research Council (CNR).

References

Allison SA, Schurr JM (1979) Torsion dynamics and depolarization of fluorescence of linear macromolecules. I. Theory and application to DNA. Chem Phys 41:35–39

Arnott S, Bond PJ (1973) Structures for poly(U) · poly(A) · poly(U) triple stranded polynucleotides. Nat New Biol 244:99–101

Barkley MD, Zimm BH (1979) Theory of twisting and bending dynamics of short linear DNAs. Analysis of triplet anisotropy decay of a 209 base pair fragment by Brownian simulation. J Chem Phys 70:2991–3007

Bonincontro A, Matzeu M, Mazzei F, Minoprio A, Pedone F (1993) Influence of defects on the electrophoretic, thermodynamic and dielectric properties of a 21 base pair DNA in solution. Biochim Biophys Acta 1171:288–294

Cantor CR, Warshaw MM, Shapiro H (1970) Oligonucleotide interactions. III. Circular dichroism studies of the conformation of deoxyoligonucleotides. Biopolymers 9:1059–1077

Collini M, Chirico G, Baldini G (1995) Influence of ligands on the fluorescence polarization anisotropy of ethidium bound to DNA. Biophys Chem 53:227–239

Duhamel J, Kanyo J, Dinter-Gottlieb G, Lu P (1996) Fluorescence emission of ethidium bromide intercalated in defined DNA duplexes: evaluation of hydrodynamics components. Biochemistry 35:16687–16697

Felsenfeld G, Davies DR, Rich A (1957) Formation of three-stranded polynucleotide molecule. J Am Chem Soc 79:2023–2024

Fujimoto BS, Millar JM, Ribeiro NS, Schurr JM (1994) Effects of different cations on the hydrodynamic radius of DNA. Biophys J 67:304–308

Gratton E, Jameson DM, Hall RD (1984) Multifrequency phase and modulation fluorometry. Ann Rev Biophys Bioeng 13:105–124

Gray DM, Ratliff RL, Vaughan MR (1992) Circular dichroism spectroscopy of DNA. Methods Enzymol 211A:389–406

Liu K, Miles HT, Parris KD, Sasisekharan V (1994) Fiber-type X-ray diffraction patterns for simple crystals of triple helical DNA. Nature Struct Biol 1:11–12

Madge D, Zappala M, Knox WH, Nordlund TM (1983) Picosecond fluorescence anisotropy decay in the ethidium/DNA complexes. J Phys Chem 87:3286–3288

Manzini G, Xodo LE, Gasparotto D, Quadrifoglio F, van der Marel G, van Boom JH (1990) Triple helix formation by oligopurine-oligopyrimidine DNA fragments. J Mol Biol 213:833–843

Mergny JL, Collier D, Rougée M, Montenay-Garestier T, Hélène C (1991) Intercalation of ethidium bromide into a triple-stranded oligonucleotide. Nucleic Acid Res 19:1521–1526

Millar DP, Robbins RJ, Zewail AH (1982) Torsion and bending of nucleic acids studied by subnanosecond time resolved fluorescence depolarization of intercalated dyes. J Chem Phys 76:4, 2080–2094

Nuutero S, Fujimoto BS, Flynn PF, Reid BR, Ribeiro NS, Schurr JM (1994) The amplitude of local angular motion of purines in DNA in solution. Biopolymers 34:463–480

Raghunathan G, Miles HT, Sasisekharan V (1993) Symmetry and molecular structure of a DNA triple helix: $d(T)_n \cdot d(A)_n \cdot d(T)_n$. Biochemistry 32:455–462

Schurr JM (1984) Rotational diffusion of deformable macromolecules with mean local cylindrical symmetry. Chem Phys 84: 71–96

Schurr JM, Fujimoto BS, Wu P, Song L (1992) Fluorescence studies of nucleic acids: dynamics, rigidities and structures. In: Lakowicz J-R (ed) Topics in fluorescence spectroscopy, vol 3. Plenum Press, New York, pp 137–229

Soyfer VN, Potaman VN (1996) Triple-helical nucleic acids. Springer, Berlin Heidelberg New York

Szabo A (1984) Theory of fluorescence depolarization in macromolecules and membranes. J Chem Phys 81:150–167

Tirado MM, Garcia de la Torre J (1980) Rotational dynamics of rigid, symmetric top macromolecules. Application to circular cylinders. J Chem Phys 73:1986–1993

Weber G (1977) Theory of differential phase fluorometry: detection of anisotropic molecular rotations. J Chem Phys 66:4081–4091